



HAL
open science

Seismic Wave Detectability on Venus Using Ground Deformation Sensors, Infrasound Sensors on Balloons and Airglow Imagers

Raphael F Garcia, Iris van Zelst, Taichi Kawamura, Sven Peter Näsholm, Anna Horleston, Sara Klaasen, Maxence Lefevre, Celine Marie Solberg, Krystyna T Smolinski, Ana-Catalina Plesa, et al.

► **To cite this version:**

Raphael F Garcia, Iris van Zelst, Taichi Kawamura, Sven Peter Näsholm, Anna Horleston, et al.. Seismic Wave Detectability on Venus Using Ground Deformation Sensors, Infrasound Sensors on Balloons and Airglow Imagers. *Earth and Space Science*, 2024, 11 (11), pp.e2024EA003670. 10.1029/2024EA003670 . insu-04771490

HAL Id: insu-04771490

<https://insu.hal.science/insu-04771490v1>

Submitted on 7 Nov 2024

HAL is a multi-disciplinary open access archive for the deposit and dissemination of scientific research documents, whether they are published or not. The documents may come from teaching and research institutions in France or abroad, or from public or private research centers.

L'archive ouverte pluridisciplinaire **HAL**, est destinée au dépôt et à la diffusion de documents scientifiques de niveau recherche, publiés ou non, émanant des établissements d'enseignement et de recherche français ou étrangers, des laboratoires publics ou privés.



Distributed under a Creative Commons Attribution 4.0 International License

Earth and Space Science



RESEARCH ARTICLE

10.1029/2024EA003670

Key Points:

- The capabilities of various measurement concepts to detect quakes on Venus are estimated and compared to recent Venus seismicity estimates
- Ground sensors are limited by their short measurement duration, but also by an atmosphere induced noise that may be above their self noise
- Atmospheric seismology concepts are limited to large quake magnitudes, and airglow imagers are favored relative to balloon measurements

Correspondence to:

R. F. Garcia,
raphael.garcia@isae-superaero.fr

Citation:


Garcia, R. F., van Zelst, I., Kawamura, T., Näsholm, S. P., Horleston, A., Klaasen, S., et al. (2024). Seismic wave detectability on Venus using ground deformation sensors, infrasound sensors on balloons and airglow imagers. *Earth and Space Science*, 11, e2024EA003670. <https://doi.org/10.1029/2024EA003670>

Received 8 APR 2024
Accepted 17 OCT 2024

Author Contributions:

Conceptualization: Raphael F. Garcia, Iris van Zelst, Krystyna T. Smolinski
Formal analysis: Raphael F. Garcia, Taichi Kawamura, Sara Klaasen
Funding acquisition: Iris van Zelst
Investigation: Raphael F. Garcia, Sven Peter Näsholm, Quentin Brissaud
Methodology: Raphael F. Garcia, Simon C. Stähler
Project administration: Iris van Zelst
Resources: Maxence Lefèvre
Software: Raphael F. Garcia, Taichi Kawamura, Sara Klaasen, Celine Marie Solberg
Validation: Maxence Lefèvre, Celine Marie Solberg, Quentin Brissaud
Visualization: Raphael F. Garcia, Sven Peter Näsholm, Sara Klaasen, Celine Marie Solberg
Writing – original draft: Raphael F. Garcia, Taichi Kawamura, Sven

Seismic Wave Detectability on Venus Using Ground Deformation Sensors, Infrasound Sensors on Balloons and Airglow Imagers

Raphael F. Garcia¹ , Iris van Zelst^{2,3} , Taichi Kawamura⁴ , Sven Peter Näsholm^{5,6} , Anna Horleston⁷ , Sara Klaasen⁸ , Maxence Lefèvre⁹ , Celine Marie Solberg⁵, Krystyna T. Smolinski⁸ , Ana-Catalina Plesa² , Quentin Brissaud⁶ , Julia S. Maia² , Simon C. Stähler⁸ , Philippe Lognonné⁴ , Mark P. Panning¹⁰ , Anna Gülcher^{10,11} , Richard Ghail¹² , and Barbara De Toffoli^{13,14} 

¹Institut Supérieur de l'Aéronautique et de l'Espace ISAE-SUPAERO, Université de Toulouse, Toulouse, France, ²Institute of Planetary Research, German Aerospace Center (DLR), Berlin, Germany, ³Centre of Astronomy and Astrophysics, Technical University of Berlin, Berlin, Germany, ⁴Université Paris Cité, Institut de physique du globe de Paris, CNRS, Paris, France, ⁵Department of Informatics, University of Oslo, Oslo, Norway, ⁶NORSAR, Kjeller, Norway, ⁷School of Earth Sciences, University of Bristol, Bristol, UK, ⁸ETH Zürich, Zürich, Switzerland, ⁹LATMOS/IPSL, Sorbonne Université, UVSQ Université Paris-Saclay, CNRS, Paris, France, ¹⁰Jet Propulsion Laboratory, California Institute of Technology, Pasadena, CA, USA, ¹¹Seismological Laboratory, California Institute of Technology, Pasadena, CA, USA, ¹²Royal Holloway, University of London, London, UK, ¹³INAF, Istituto di Astrofisica e Planetologia Spaziali, Rome, Italy, ¹⁴Department of Geosciences, University of Padova, Padova, Italy

Abstract The relatively unconstrained internal structure of Venus is a missing piece in our understanding of the formation and evolution of the Solar System. Detection of seismic waves generated by venusquakes is crucial to determine the seismic structure of Venus' interior, as recently shown by the new seismic and geodetic constraints on Mars' interior obtained by the InSight mission. In the next decade multiple missions will fly to Venus to explore its tectonic and volcanic activity, but they will not be able to conclusively detect seismic waves, despite their potential to detect fault movements. Looking toward the next fleet of Venus missions after the ones already decided, various concepts to measure seismic waves have been proposed. These detection methods include typical geophysical ground sensors already deployed on Earth, the Moon, and Mars; pressure sensors on balloons; and imagers of high altitude emissions (airglow) on orbiters. The latter two methods target the detection of the infrasound signals generated by seismic waves and amplified during their upward propagation. Here, we provide a first comparison between the detection capabilities of these different measurement techniques and recent estimates of Venus' seismic activity. In addition, we discuss the performance requirements and measurement durations required to detect seismic waves with the various detection methods. Our study clearly presents the advantages and limitations of the different seismic wave detection techniques and can be used to drive the design of future mission concepts aiming to study the seismicity of Venus.

Plain Language Summary We do not really know what the interior of Venus looks like. Even the first-order structure of the size of Venus' core is plagued with large uncertainties. For other planets, such as the Earth and Mars, the interior structure is much better constrained. This is largely thanks to the seismological investigations performed on these planets that revealed their interior structure by studying the seismic waves caused by quakes. In the next decade, new missions will fly to Venus to explore its tectonic and volcanic activity, which is interesting to estimate seismicity. But these missions will not be able to detect any seismic waves. In order to help design future mission concepts, we discuss instruments that could record seismic waves, as already used on the Earth, the Moon, and Mars; instruments on balloons that could float in the Venusian atmosphere; and instruments on spacecrafts that monitor the variations of atmospheric emissions caused by seismic waves originating at the surface. We compare all these different techniques with each other and with recent estimates of Venus' seismic activity to see which of them works best in different scenarios.

© 2024. The Author(s).

This is an open access article under the terms of the [Creative Commons Attribution License](https://creativecommons.org/licenses/by/4.0/), which permits use, distribution and reproduction in any medium, provided the original work is properly cited.

1. Introduction

The formation and the evolution of our Solar System is informed by the internal structures of the rocky planets. Although Venus is similar to Earth in terms of size and mass, we do not have a good understanding of Venus'

Peter Näsholm, Anna Horleston,
Sara Klaasen, Maxence Lefèvre, Krystyna
T. Smolinski, Quentin Brissaud
Writing – review & editing: Raphael
F. Garcia, Iris van Zelst, Sven
Peter Näsholm, Maxence Lefèvre,
Krystyna T. Smolinski, Ana-
Catalina Plesa, Quentin Brissaud, Julia
S. Maia, Simon C. Stähler,
Philippe Lognonné, Mark P. Panning,
Anna Gülcher, Richard Ghail,
Barbara De Toffoli

interior because we do not have any seismic observations. Without such observations, geodetic observations are also limited due to the slow rotation of Venus, which hinders the determination of its moment of inertia (Margot et al., 2021) and leads to large uncertainties in Love number estimates (Dumoulin et al., 2017). The detection and characterization of seismic waves is the best tool to infer the internal structure of planets (Lognonné et al., 2023). However, the deployment of long-duration geophysical instrumentation, which demonstrated its capabilities during the InSight mission on Mars (Drilleau et al., 2022; Durán, Khan, Ceylan, Charalambous, et al., 2022; Durán, Khan, Ceylan, Zenhäusern, et al., 2022; Lognonné et al., 2023; Samuel et al., 2023; Stähler et al., 2021) is not possible on Venus due to its harsh surface conditions. At the same time, there is a growing number of studies that have presented evidence that Venus is volcanically and tectonically active at present (Byrne et al., 2021; Gülcher et al., 2020; Herrick & Hensley, 2023; Smrekar et al., 2010, 2023; van Zelst, 2022) indicating that the planet is probably also seismically active. Indeed, recent estimates of Venus' seismicity indicate that Venus could host hundreds of quakes per year with $M_w \geq 5$ when Venus is assumed to be moderately active, and could potentially be as seismically active as the Earth (van Zelst et al., 2024).

Despite the compelling arguments in favor of monitoring seismic wave propagation in Venus, none of the three missions scheduled by ESA and NASA to visit Venus in the next decade (i.e., the EnVision (Widemann et al., 2022), VERITAS (Smrekar et al., 2022), and DAVINCI+ (Garvin et al., 2022) missions) are targeting the detection of seismic waves. This is primarily due to the challenges associated with conducting such measurements for Venus. Over the past decade, various measurement concepts have been explored, falling into three main categories: (a) ground deformation instruments deployed on the planet's surface, (b) infrasound sensors mounted on balloon platforms, and (c) airglow imagers on board orbiters (Stevenson et al., 2015). The concepts for ground surface deployment of seismic sensors are limited by the high atmospheric surface temperature (≈ 740 K) and the absence of high temperature electronics. This limits the measurement duration to a total of less than 24 hr (Beauchamp et al., 2021; Kremic et al., 2020). Seismic infrasound detection methods benefit from the low attenuation of upward-propagating infrasound waves created by seismic waves below 1 Hz (Garcia et al., 2005). These infrasounds conserve the dispersion features of seismic surface waves during their upward propagation (Garcia et al., 2022; Lognonné et al., 2016). These two properties allow us to assume that the infrasound created by seismic surface waves retains all the properties of seismic surface waves. Thus allowing us to determine the seismic velocity profile in the first hundreds of kilometers depth of the planet, as it was done by InSight on Mars (Carrasco et al., 2023; Kim et al., 2022; Xu et al., 2023). Two different concepts based on the detection of seismic infrasound have been investigated thoroughly in the past decade. First, pressure sensors on board balloon platforms have been studied (Krishnamoorthy & Bowman, 2023; Stevenson et al., 2015). Their capabilities to detect and characterize seismic waves have been demonstrated theoretically and have even been observed on Earth recently for the first time (Brissaud et al., 2021; Garcia et al., 2022; Gerier et al., 2024). Secondly, airglow emission variations induced by seismically generated tsunami waves have been observed on Earth (Makela et al., 2011; Occhipinti et al., 2011) and the sensitivity of airglow emissions to gravity waves has been observed in Venus' atmosphere (Garcia et al., 2009). Indeed, mission concepts targeted to the observation of seismically induced variations of 1.27 μm nightglow and 4.3 μm dayglow in Venus' atmosphere have been developed (Stevenson et al., 2015; Sutin et al., 2018).

The purpose of this study is to perform a first comparison between the capabilities of these diverse measurement techniques and the most recent estimates of Venus seismicity. For each observation technique, we also discuss the minimum performance and measurement duration. We focus on globally observable seismic waves for events of moment magnitude larger than 3 ($M_w > 3$).

2. Estimating Seismic Wave Detection Capabilities of Different Observation Concepts

2.1. Seismic Signal Estimates

In the absence of internal structure models of Venus that are directly constrained by data, the currently used internal structure models of Venus are constrained by planetary formation and geodynamic models, solar abundance estimates, and physical assumptions, and rely on the adaptation of Earth models to Venus conditions (Gudkova & Zharkov, 2020; Zharkov, 1983). As a consequence, these models present a large uncertainty in terms of both seismic velocities and seismic attenuation parameters. This is why we choose to base our estimates of seismic wave amplitudes and frequency content on Earth's scaling relations, rather than performing complex computations in highly uncertain models of the Venusian interior. Because seismic surface waves show the

highest amplitude for shallow quakes on Earth, we will assume that these waves are also dominating the seismic signal on Venus in the quake magnitude range considered in this study, that is, moment magnitudes larger than 3.0. We also focus on seismic surface waves because their dispersion can be measured on a single record and informs on the structure of the first hundreds of kilometers of Venus' interior. The definition of surface-wave magnitude, M_S , shows a direct link with the amplitude of the seismic surface Rayleigh waves around the 20 s period:

$$M_S = \log_{10}\left(\frac{A_d}{T_S}\right) + 1.66\log_{10}(\Delta) + 3.3, \quad (1)$$

where M_S is the surface wave magnitude, A_d the vertical ground displacement in μm , T_S is the period considered for measuring A_d , and Δ is the epicentral distance of the quake in degrees (Bormann & Dewey, 2012). We will use this relation to determine the amplitude of the surface Rayleigh waves as a function of distance for a given surface wave magnitude.

2.2. Atmosphere Effects and Parameters

The detectability of infrasound by balloon platforms and airglow imagers is sensitive to the amplitude of the source and atmospheric path effects (Garcia et al., 2005). In particular, attenuation processes on Venus can strongly dampen and disperse the infrasound energy. To assess the impact of attenuation on acoustic waves, we determine the energy loss versus altitude for a vertically propagating planar wave. In the frequency range (0.02–10 Hz), the attenuation of infrasound in the Venusian atmosphere is dominated by CO_2 relaxation effects (Bass & Chambers, 2001; Petculescu, 2016), although some contributions are also expected from sulfuric acid (H_2SO_4) droplet-related processes, primarily in the cloudy 45–70 km altitude range (Trahan & Petculescu, 2020).

We compute atmospheric parameters using the Venus Climate Database (VCD) (Gilli et al., 2017, 2021; Martinez et al., 2023) to estimate the attenuation due to CO_2 relaxation, $\alpha_{\text{CO}_2}(z)$. We extract a single vertical profile of specific heats, and sound speed is extracted at the equator at midday local time. From this VCD profile, we then use the approach described in Garcia et al. (2017) to extract the CO_2 relaxation frequency and relaxation strength, as well as the sound speed as a function of altitude. In low-attenuation scenarios, it is appropriate to sum the attenuation contributions from CO_2 and H_2SO_4 (Nachman et al., 1990), to obtain the total attenuation $\alpha_{\text{tot}}(z) = \alpha_{\text{CO}_2}(z) + \alpha_{\text{H}_2\text{SO}_4}(z)$. In Figure 1, we use these estimates to explore the amplitude loss using a plane-wave assumption, focusing on acoustic waves at periods from 0.1 to 50 s from the ground up to 140 km altitude. A significant increase in attenuation occurs in the cloud layers, where strong diffusion-mediated phase changes occur due to sulfuric acid droplets (Petculescu, 2016). Yet, our estimates suggest that attenuation has an insignificant impact on acoustic waves of periods larger than 1 s up to the bottom of the airglow layer IR1. At the altitude of airglow layer IR2, longer-period waves of interest for airglow (10–50 s period) are not damped much. However, at this altitude, a significant energy loss of $\sim 50\%$ is predicted for the shorter-period, higher-frequency waves, which dramatically reduces the likelihood of detection for 1 s period waves. In contrast, at balloon altitudes, acoustic waves generated by ground movements can be observed to 10 Hz, which is interesting for the observation of small-magnitude quakes. Note that this analysis assumes linear acoustics and takes neither nonlinear propagation nor wave-breaking effects into account.

2.3. Estimating the Minimum Number of Events Per Magnitude Per Year

In this section, we provide detection thresholds that can be directly compared to seismicity estimates (van Zelst et al., 2024). To do so, we estimate the requirements to detect at least one event larger than a given magnitude during the full mission duration. This requirement yields the following relation for a signal-to-noise ratio threshold of one:

$$N_m^{\text{min}}(M_S) = \frac{1}{T_m} \frac{S_P}{S_m(M_S)}, \quad (2)$$

where $N_m^{\text{min}}(M_S)$ is the minimum number of seismic events of surface wave magnitude larger than M_S required to detect at least one by a given method, T_m is time in Earth years, S_P is the surface area of Venus, and *_m signifies

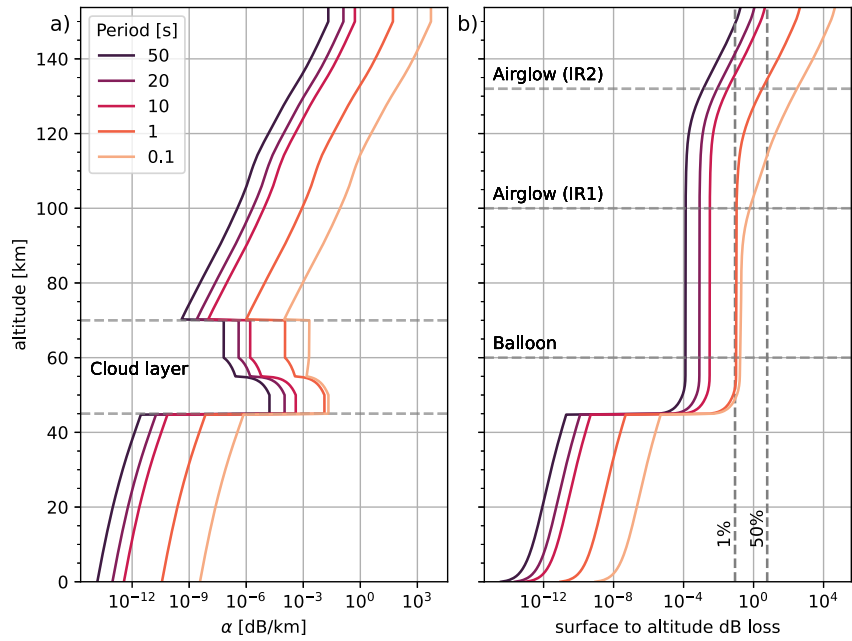


Figure 1. (a) Plane-wave infrasound attenuation (α in dB/km) based on a Venus Climate Database (VCD) atmospheric profile, including both the $\alpha_{\text{H}_2\text{SO}_4}$ and the α_{CO_2} contributions, and the sulfuric acid cloud contributions given in Trahan and Petculescu (2020). We consider wave periods from 0.1 to 50 s. (b) The total loss (in dB) due to the attenuation in (a), integrated from the ground up to the given altitude. The two vertical dashed lines indicate accumulated amplitude losses of 1% and 50%.

method m : s for seismometer, r for ground rotation sensor, d for ground Distributed Acoustic Sensing (DAS), b for pressure sensors on board balloons and a for airglow imagers. Note that for airglow imagers this relation is valid only for a single pixel of the airglow image. In this relation, the surface area $S_m(M_S)$ over which a quake of a given surface-wave magnitude M_S can be detected by a given method is investigated in the following sections.

This relation is only statistically valid with a 63% confidence interval, if we assume that the seismic events have a Poisson distribution. Moreover, it is assumed that the seismic event probability is homogeneous over the Venus surface, which is unrealistic, but a starting point at a time when no actual mission concept has been evaluated. Our estimates thus provide a lower bound of the detection limits of each measurement concept.

In order to estimate $\frac{S_p}{S_m(M_S)}$, we need to estimate a maximum distance $\Delta_m(M_S)$, usually in degrees, at which the event can be detected for the different methods, within a signal-to-noise ratio larger than a given value SNR_{\min} . Knowing this number, the surface area ratio is

$$\frac{S_p}{S_m(M_S)} = \frac{4\pi}{2\pi(1 - \cos(\Delta_m(M_S)))}, \quad (3)$$

with $\Delta_m(M_S)$ the maximum epicentral distance at which you can expect to detect the quake.

Usually, the noise levels of the instruments are provided in Power of Amplitude Spectral Density (ASD) in physical unit over square root of hertz (ASD_n). In contrast, the signal amplitude terms in Equation 1 are provided at a given period (T_S), and consequently the signal amplitude on the instrument is also in physical units at a given period (A_m). In order to compare these two numbers, we convert the ASD values into root-mean-square values, under the conservative hypothesis that we filter the signals over a bandwidth of 1/3 octave ($\pm 11.5\%$) around the central frequency $f_S = \frac{1}{T_S}$. As a consequence, the root-mean-square noise amplitude is defined by the product of the ASD times the square root of the frequency bandwidth, assuming that the noise power is constant over the bandwidth (Bormann, 2002):

$$N_{rms} = ASD_n \sqrt{\frac{0.23}{T_s}}. \quad (4)$$

As a consequence, the maximum epicentral distance at which you can expect to detect a quake of magnitude M_S ($\Delta_m(M_S)$) is defined by equating the signal-to-noise ratio to its minimum value SNR_{min} , fixed here to 3:

$$\frac{A_m(\Delta_m(M_S))}{N_{rms}} = SNR_{min}. \quad (5)$$

In conclusion, in order to estimate $N_m^{min}(M_S)$, that is, the minimum number of events per year, as a function of surface wave magnitude, to measure at least 1 event of this type by a given method, one needs to invert the above equations to get the maximum distance at which an event can be detected by a given method $\Delta_m(M_S)$, and then compute $N_m^{min}(M_S)$ through Equations 3 and 2. However, because the relation of Equation 1 holds only for teleseismic distances, and because we need the waves to be separated in time in order to analyze them properly, we impose $\Delta_m(M_S) > 3^\circ$. This restriction sets the lower-bound limit on the M_S values.

These relations apply strictly to single point measurements like ground and balloon measurements. For airglow imagers, this relation applies to each pixel of the airglow image but the detection capabilities for the whole image needs more assumptions and analysis that are presented in detail in Section 2.4.5.

2.4. Detection Capabilities of Various Observation Concepts

2.4.1. Quake Detection by Landed Seismometer

2.4.1.1. Technological Assumptions

Due to the high surface temperatures on Venus and the limited amount of solar energy that reaches the surface, deploying instruments on the ground is challenging. With conventional electronics, surface landers lasted less than 2 hours on the Venusian surface in the past (Kerzhanovich & Marov, 1983; Moroz, 1983).

Recent advances in high-temperature electronics (Glass et al., 2020; Kremic et al., 2020; Wilson et al., 2016) have made long-lived landers a possibility for the coming decades, using silicon carbide (SiC) seismometers. These SiC integrated circuits have been demonstrated to provide 60 functioning days in high-fidelity simulated Venusian surface conditions (Chen et al., 2019; Hunter et al., 2021; Neudeck et al., 2018). However, the development of the associated electronics to cope with the harsh Venus conditions is still required. Memory is another issue with Venusian surface conditions. Depending on power availability, data storage and transmission could be difficult. Tian et al. (2023) designed a low-memory algorithm to circumvent this issue that triggers transmission during earthquakes and avoids transmission during wind and other noise events.

Despite these encouraging technological developments we will assume that ground sensors of future missions will operate with their associated electronics inside a thermally insulated lander. This assumption limits the observation time to about 12 hr, which is a compromise between the values provided by Kremic et al. (2020) (24 hr) and Beauchamp et al. (2021) (6–8 hr).

2.4.1.2. Background Noise of Ground Sensors

Ground sensors will be impacted by both the harsh surface environment and noise sources coming from the atmosphere dynamics. A thorough analysis of these noise sources requires the production of a noise model (Mimoun et al., 2017; Pinot et al., 2024). However, an order of magnitude computation of the Brownian thermal noise acting on the mass/spring system of the seismometer indicates that this noise source is below $10^{-8} \text{ m/s}^2/\sqrt{\text{Hz}}$. Other instrument noise sources should also be considered and properly calculated for the Venusian environment, such as digitizer/acquisition noise, thermal noise, wind noise on the sensor and on the landing system, but such computations require knowledge of the instrument and landing systems. However, we try in the next paragraphs to estimate the atmospheric noise contribution from the wind, which we estimate to be dominant above other noise sources.

Only a handful of probes have recorded atmospheric data at the surface of Venus. Only VENERA-9 and 10 directly measured the wind for 49 min and 90 s, respectively (Avduevskii et al., 1977), and VENERA-13 and 14 indirectly measured the wind speed (Ksanfomaliti et al., 1983). The amplitudes of the measured wind speeds are less than 2 m s^{-1} below 100 m height (Lorenz, 2016), with a higher probability for values below 0.5 m s^{-1} .

Simulations with a global circulation model showed that the diurnal cycle of the Planetary Boundary Layer (PBL) activity is correlated with the diurnal cycle of surface winds (Lebonnois et al., 2018), with downward katabatic winds at night and upward anabatic winds during the day along the slopes of high-elevation terrains. With a high-resolution model, Lefèvre et al. (2024) confirmed this diurnal cycle of the surface wind. The resolved large-scale horizontal wind at 10 m above the local surface is above 1 m s^{-1} in the mountains in the equatorial region and below 0.5 m s^{-1} in the low plains.

Lefèvre (2022) used a turbulent-resolving model to quantify the turbulent activity at the surface of Venus. At noon, the height of the PBL varies from 1.5 km in the plains to 7 km in the high terrains by the equator. This difference is due to the impact of the anabatic winds. This difference in PBL height at noon results in a difference in the amplitude of turbulent horizontal winds, reaching 2 m s^{-1} for the high terrain compared to between 1 and 1.5 m s^{-1} in the plains. At night, when the impact of the slope winds is weaker, the height of the PBL is almost the same (around 500 m), resulting in a horizontal wind amplitude below 0.5 m s^{-1} . Placing a seismometer in the low plain, and recording signals at night, seems to be the optimal plan to limit the noise of the atmosphere.

Lorenz (2012) roughly quantified the wind noise at the surface of Venus. With an atmospheric density of 65 kg/m^3 , a wind speed of 0.25 m s^{-1} is comparable in terms of dynamic pressure to wind speeds of 20 m s^{-1} on Mars, which were regularly observed during the daytime by InSight (Banfield et al., 2020). The corresponding seismic amplitude is 120.0 nm.

Venera-14 reportedly detected Venusian microseisms with a geophone in only one hour of operation (Ksanfomaliti et al., 1982). The amplitude of the signals are consistent with “noisy” environments on Earth (Lorenz & Panning, 2018), that is, from $\sim 10^{-8}$ to $10^{-6} \text{ m/s}^2/\sqrt{\text{Hz}}$ which roughly spans the space between the low and high noise models for Earth (Peterson, 1993). We will use these values for all ground sensors and compare these with instrument self noise when available.

It is important to note that for high-quality ground vibration measurements, the ground sensors will need to be protected from the wind, and the wind speed and pressure should be monitored continuously, as already performed by the InSight mission (Lognonné et al., 2019).

2.4.1.3. Estimates of Detection Capabilities

With an SNR_{\min} set to 3 and a period T_s of 20 s, $\Delta_m(M_S)$ can be estimated for a given magnitude from Equations 1 and 5 as:

$$\log_{10}(\Delta_m(M_S)) = \frac{M_s - 3.3 - \log_{10}\left(\frac{\text{SNR}_{\min} N_{rms}}{T_s}\right)}{1.66}. \quad (6)$$

Following Equations 2 and 3, the minimum number of events for each magnitude on the surface of Venus needed to obtain at least one detection during the mission lifetime is shown in Figure 2. For the lowest noise level, estimated to be $10^{-8} \text{ m/s}^2/\sqrt{\text{Hz}}$ (low noise sensor, protected from wind, on a hard surface), global detection is possible for surface wave magnitudes above $M_s = 4.3$. For a higher noise level, this limit increases to $M_s = 5.3$ for $10^{-7} \text{ m/s}^2/\sqrt{\text{Hz}}$ (low noise sensor, protected from wind, on a soft surface) and to $M_s = 6.3$ for $10^{-6} \text{ m/s}^2/\sqrt{\text{Hz}}$ (sensor unprotected from wind). Under our idealized conditions, events above this threshold need to occur just once during the mission to be detectable. This gives the lower limit of 730 events per year in Figure 2.

2.4.2. Quake Detection With DAS on the Surface

Distributed Acoustic Sensing (DAS) is an emerging technology in the field of Earth geophysics, and has been applied in increasingly remote and harsh locations on Earth, such as glaciers (Hudson et al., 2021; Walter et al., 2020), volcanoes (Jousset et al., 2022; Klaasen et al., 2021, 2023) and submarine environments (Cheng

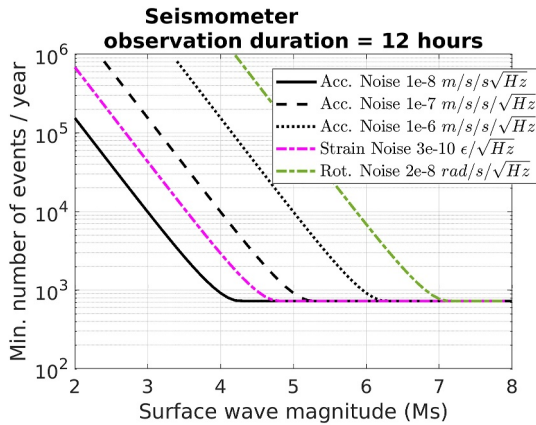


Figure 2. Minimum number of events per year as a function of surface wave magnitude required on the surface of Venus to measure at least one event of this magnitude during a ground instrument observation duration of 12 hr. Results are provided for different seismometer noise levels in acceleration: 10^{-8} (plain line) and 10^{-7} (dashed line), 10^{-6} (dotted line) $\text{m/s}^2/\sqrt{\text{Hz}}$ at 20 s period. Estimates for Distributed Acoustic Sensing strain sensors with a self noise level of $3 \times 10^{-10} \epsilon/\sqrt{\text{Hz}}$ (dotted-dashed magenta line) and ground rotation sensors with a self noise level of $2 \times 10^{-8} \text{rad/s}/\sqrt{\text{Hz}}$ are also provided and discussed in Sections 2.4.2 and 2.4.3 respectively.

in strain as reported by the iDAS Carina from Silixa, as an example of the self-noise of an interrogator currently on the market.

While the calculation based on different noise estimates paints an optimistic picture, we emphasize that a DAS deployment on Venus is not yet feasible due to several obstacles, such as (a) the current instrumental capacities, (b) deployment options, (c) cable coupling conditions, and (d) unknown cable locations. The instruments currently on the market are not able to operate under the pressure and temperature at the surface of Venus. However, some experiments have demonstrated the ability of specialized gold-coated optical fibers to survive and function with low attenuation at temperatures up to 773 K for up to 900 hr (Jacobsen et al., 2018), with optical fiber manufacturers also quoting operating temperatures up to 973 K (e.g., (Heracle, 2023)). The development of high-temperature and corrosion-resistant fibers is an area of active research, for example, within the oil and gas industry (Reinsch & Hennings, 2010; Stolov & OFS, 2019). Alternative fiber optic sensing systems are also already in development for structural health monitoring on future spacecraft (Chan et al., 2015; Parker et al., 2024).

Even if a DAS cable were able to operate on the surface of Venus, we would be limited by the deployment of the cable. If the cable is released during the landing, we are unable to control the exact layout and coupling conditions of the cable, which will likely decrease the data quality and the consequent conclusions that can be drawn from the data. If the cable is not buried and protected, other noise sources are likely to overpower any seismic signals—a phenomenon observed on Earth with atmospheric noise, in submarine environments with strong currents (Lior et al., 2021), or on Mars with the atmospheric wind and pressure noise (Mimoun et al., 2017). Additionally, DAS yields single-component data, therefore a cable layout with varying angles and directions is necessary to capture the complete wavefield and locate events. However, this also requires exact geographical knowledge of the cable layout, which may be difficult to obtain on Venus due to the lack of a GPS network and difficulty capturing georeferenced images of the cable.

Hence, in order to facilitate a DAS experiment on Venus, research primarily needs to focus on instrumental development and the feasibility of experimental deployment. The instrument needs to be able to operate its laser and conduct preliminary data analysis before sending the data back to orbit in order to avoid a bottleneck caused by the large amounts of data produced during DAS experiments. Additionally, the cable needs to be deployed in such a fashion to guarantee atmospheric protection, good coupling with the ground, and a well-known, non-linear layout.

et al., 2021; Lior et al., 2021). It employs a fiber-optic cable that is interrogated with laser pulses, resulting in seismic deformation measurements at a high spatial and temporal resolution along the cable. We refer the reader to Zhan (2020), and Lindsey and Martin (2021) for more in-depth descriptions of DAS and its applications on Earth. We optimistically propose to extend the use of DAS beyond Earth, and to visualize the hypothetical detection capabilities of DAS on Venus.

We follow the procedures outlined in Section 2.3 to obtain the detection capabilities of DAS on Venus. We estimate the minimum number of required events per year based on parameters and assumptions similar to those used for the landed seismometer in Section 2.4.1. The noise estimates in $\text{m/s}^2/\sqrt{\text{Hz}}$ can be transformed from ground acceleration to strain, and vice versa, using the plane-wave assumption (Daley et al., 2016; Näsholm et al., 2022; Wang et al., 2018), assuming an apparent velocity of seismic surface waves of 2250 m/s, which corresponds to an approximate Rayleigh wave velocity in mid-oceanic ridge basaltic material at 20 s period (as suggested for Venus; Surkov et al., 1984) with a Poisson ratio of 0.25:

$$\epsilon = aT_S/V_R, \quad (7)$$

where ϵ is the strain, a is the acceleration in m/s^2 which is linked to a given quake magnitude by Equation 1, T_S is the period of the wave in s, and V_R is the Rayleigh wave velocity in m/s. Figure 2 shows the results for the noise-floor

2.4.3. Quake Detection With Ground Rotation Sensors

The sensing of the ground rotations induced by seismic waves is an emerging field. Knowledge of ground rotations allow one to infer the gradients of the seismic wavefield. These measurements allow seismologists to distinguish between various seismic waves (Sollberger et al., 2023), to correct for tilt effects on seismometers (Bernauer, Wassermann, & Igel, 2020) and to infer anisotropy parameters (Noe et al., 2022). There are also many other applications for inverse problems and seismic source determination (Schmelzbach et al., 2018). This domain is currently limited by the self-noise level of the instruments (Bernauer et al., 2021) and planetary applications are promising but mainly limited by the available instrumentation (Bernauer, Garcia, et al., 2020).

Currently available instruments measure the ground rotation speed in rad/s (ω) along three perpendicular axis. With the same assumption as those used in the previous section to estimate the ground strain, this parameter can be linked to the ground acceleration using the following equation

$$\omega = aT_S/(2\pi\lambda), \quad (8)$$

where ω is the ground rotation in rad/s, a the acceleration in m/s^2 , T_S the period of the surface wave in s, and λ the wavelength in meters which is computed assuming a surface wave velocity of 2250 m/s.

We follow the procedures as outlined in Section 2.3 to obtain the detection capabilities for ground rotation sensors on Venus. We estimate the minimum number of required events per year based on parameters and assumptions similar to the ones used for the landed seismometer in Section 2.4.1. Figure 2 shows the results for the noise-floor in rad/s as reported for the BlueSeis3A sensor from the company iXblue ($20 \text{ nrad/s}/\sqrt{\text{Hz}}$), as an example of the self-noise of a rotation sensor on the market.

As observed in Figure 2, the event detection is limited by the self-noise of current ground rotation instruments (Bernauer, Garcia, et al., 2020). Ground rotation measurement systems present deployment constraints similar to the ones of a seismometer but excluding the need for leveling for systems based on fiber optics gyroscopes. Even if these deployment constraints are less stringent than the ones of DAS systems, the interest of such measurements is limited to large-amplitude signals, and thus to large-amplitude quakes close to the instrument.

2.4.4. Quake Detection by Pressure Sensors Onboard Balloons

Balloons have already flown in Venus' atmosphere at about 54 km altitude for more than 45 hr in the framework of the USSR VEGA missions (Sagdeev, 1986; Sagdeev, Linkin, Lipatov, et al., 1986). Their instrumentation (Kremnev et al., 1986) recorded pressure and temperature (Sagdeev, Linkin, Kerzhanovich, et al., 1986), which allowed the estimation of vertical wind speeds. Balloon platforms have various advantages for the detection of infrasound generated by quakes. First, they operate in an altitude range (inside or above Venus' clouds) for which temperatures and pressures are comparable to those at Earth's surface, thus avoiding the need for very high temperature technologies. Secondly, because balloons drift with the background winds, the relative wind between the sensor and the atmosphere is small, as is the corresponding wind noise. Recent proposals for Venus balloon missions estimate that their trajectory will complete one orbit of the whole planet at the equator in five to 6 days, with a latitude varying from one circuit or the other (Beauchamp et al., 2021). The mission duration is estimated between 60 days for the Venus Flagship Mission (Beauchamp et al., 2021) and 117 days for the ADVENTS mission concept (O'Rourke, 2021). We chose 3 months (90 days) for balloon observation duration as a compromise between these two values.

Stratospheric balloon flights in Earth's lower stratosphere experience noise levels around $0.05 \text{ Pa}/\sqrt{\text{Hz}}$ at 20 s period and $0.01 \text{ Pa}/\sqrt{\text{Hz}}$ at 10 s period (Garcia et al., 2022). We expect similar background noise levels to occur above the convective cloud regions in Venus' atmosphere as these altitudes are also dominated by laminar flows presenting similar vertical wind shear.

The amplitude of pressure perturbations generated by a vertical displacement A_d (in μm) at period T_S can be computed using the following formula, assuming that the acoustic wave attenuation is negligible (Garcia et al., 2005):

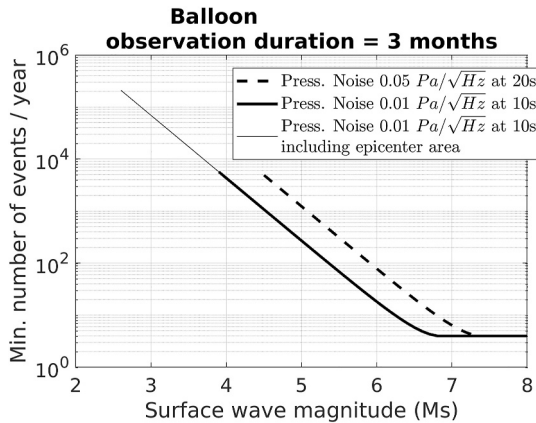


Figure 3. Minimum number of events per year as a function of surface wave magnitude required to measure at least one event of this magnitude during a balloon mission duration of 3 months. Results are provided at two different periods: 20 s (thick dashed line) and 10 s (thick plain line) because the noise level of pressure measurements varies significantly with frequency (from 0.05 to 0.01 Pa/√Hz going from 20 to 10 s period). We also show the results for a noise level of 0.01 Pa/√Hz at 10 s period but with the minimum distance between quake and sensor reduced from 3° to 0.5° (thin solid line).

corresponding result is shown as a thin line in Figure 3. It demonstrates that balloons can detect quakes of surface wave magnitudes as small as 2.6 at distances less than 55 km from the source, as already observed on Earth (Brissaud et al., 2021; Krishnamoorthy et al., 2023). However, this range of distance and magnitude is outside the range of validity of our Equation 1. This is why we will retain only results for a minimum distance of 3° between the sensor and the quake.

2.4.5. Quake Detection by Airglow Measurements Onboard Orbiters

The airglow emissions are upper atmosphere emissions generally induced by the night side recombinations of molecules that were dissociated on the day side by solar radiation. The emitted photons are at a given wavelength imposed by the molecular reaction mechanism. Various studies pointed to the sensitivity of Venus' airglow emissions to pressure, temperature and density variations induced by acoustic waves (Garcia et al., 2009; López-Valverde et al., 2011; Stevenson et al., 2015). These studies mainly target two infrared airglows: nighttime airglow at 1.27 μm and day time Non-Local Thermodynamical Equilibrium emissions around 4.3 μm (in fact two emission peaks at 4.28 μm and 4.32 μm).

The night side airglow at 1.27 μm is due to the recombination of oxygen atoms. The emission layer is peaking around 100 km altitude (Gérard et al., 2008) and presents large longitudinal and latitudinal variations (Gérard et al., 2014), as well as a natural time variability over time scales of around 1000 s. However, it is predicted to react almost instantaneously to the density and temperature variations expected from seismic infrasounds (Sutin et al., 2018).

The day time airglows at 4.28 μm and 4.32 μm peak respectively around 135 and 140 km (Garcia et al., 2009). They are induced by a mechanism different to the one usually generating airglow emissions. These emissions are due to the natural return to a lower energy state of CO₂ molecules after excitation by solar radiation (López-Valverde et al., 2011) and without involving any collisions with other molecules. The background emission varies smoothly as a function of solar illumination (solar zenith angle). These emissions are sensitive to density and temperature variations that are changing the collision rate of the molecules, as already observed for gravity wave perturbations in Venus' atmosphere (Garcia et al., 2009).

Previous studies paved the way for a dedicated mission concept studied at JPL/NASA (Sutin et al., 2018). We will use this mission design, called VAMOS, in order to infer the detection capabilities of airglow measurements in terms of the minimum number of events per year required to detect at least one quake with this detection method. The concept is targeting a continuous monitoring of the planet disk with a high sampling rate (>1 sample per

$$DP = \rho(z_b) c(z_b) \sqrt{\frac{\rho(0)}{\rho(z_b)}} \left(\frac{2\pi 10^{-6} A_d}{T_S} \right) \quad (9)$$

in which $\rho(z)$ and $c(z)$ are the density and the sound speed at altitude z in the atmosphere respectively. The product of the first two terms is the impedance conversion from vertical particle velocity to pressure at balloon altitude ($z_b = 60$ km). The third term is the amplification factor for particle velocity from the ground to the balloon altitude. The last term is the ground vertical velocity of seismic waves in m/s at T_S period.

Using Equations 2–6 and 9 one can obtain the minimum number of events per year required to measure at least 1 event of a given magnitude during the observation duration. The results are presented in Figure 3. This suggests a minimum number of events with $M_S = 6$ between 20 and 100 is required to detect at least one quake. Note that at large magnitudes, the minimum number of events is limited to 4 per year, because the mission duration is 1/4 of a year. Extending the mission duration would lower this flat part of the curve and extend further the part of the curve with a negative slope in the direction of high magnitudes.

In order to infer the capability of balloons to detect small quakes close to the epicenter, we reduced the minimum distance to the epicenter to 0.5°. The

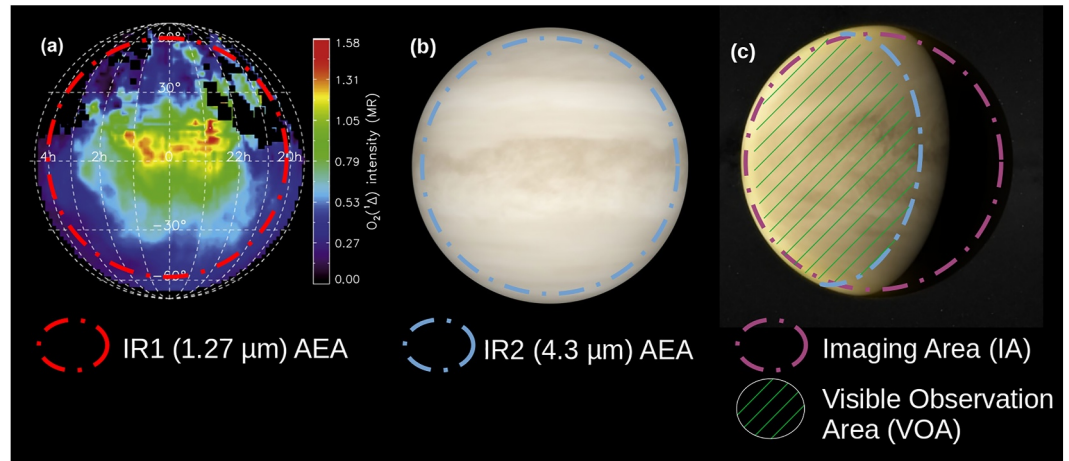


Figure 4. Definitions of Aiglow Emission Areas (a) and (b), Imaging Area (IA) (c) and Visible Observation Area (VOA) (c). (a) IR1 (1.27 μm) Airglow Emission Area (AEA) on top of night side 1.27 μm radiance estimates by Soret et al. (2012), (b) IR2 (4.3 μm) AEA on top of an optical image of Venus' day side, and (c) definition of IA and VOA on top of an optical image of Venus.

second) camera orbiting on a circular equatorial orbit at a radius of 45,000 km with a period of approximately 29.2 hr. The observation duration is extracted from this mission concept and is set to 2 years.

As the measurement concept is different from a single point measurement by landed seismometers or balloons, Equations 2–6 must be revised because they are valid only for single pixels in the image, not for the whole image. First, because the airglow emissions are localized only on a specific part of the planet, we must define this area as the Airglow Emission Area (AEA) for a given airglow. For the 1.27 μm emission, this observation area is centered on the equatorial point at 0:00 a.m. local time and covers an angular radius of about 60° around that point, because it is in this region that we expect the largest background emissions (Gérard et al., 2008; Soret et al., 2012). For simplicity, we assume that the center point of this area is located at midnight local time.

For the 4.3 μm emission, the observation area is centered on the equatorial point at 12:00 local time (midday) and covers an angular radius of about 70° around that point. These emissions are proportional to solar illumination, but polar regions and regions close to the terminator are conservatively excluded because background emissions are low, and because more variability is expected from gravity wave activity (García et al., 2009; Gérard et al., 2014; Seiff & Kirk, 1991).

Another difference compared to single point measurements is that the AEA is not always visible in the camera images. To illustrate this, we use the equatorial circular orbit of VAMOS to simplify the computations, although it still provides similar visibility statistics to other orbits at different ellipticity and inclination when ensuring that the full disk is visible on more than 80% of the orbit period. In the full-disk images of the planet, we conservatively consider that only points having an angular distance smaller than 70° for the center of the image (located at the equator) can be used for observation because points close to the limb will have too much image distortion. This region of the image is named the Imaging Area (IA). As a consequence, for a given local time position (ϕ in longitude degrees) of the center of the IA (at the equator) relative to the center position of the AEA (ϕ_0) the Visible Observation Area (VOA) will be defined by the intersection of two spherical caps (or solid angles) of size 60° (or 70°) for the AEA and size 70° for the IA. Due to the rotation of the spacecraft around the planet, the size of the VOA will vary as a function of the parameter ϕ . The definitions of AEA, IA and VOA are summarized in Figure 4.

The function $\text{VOA}(\Delta\phi)$, with $\Delta\phi = \phi - \phi_0$, is symmetric around zero. When this area is zero (i.e., the AEA is not visible from the spacecraft) the corresponding time period must be subtracted from the mission duration to define the observation duration (T_m of Equation 2). When this area is non-zero, all the points in the area have the capability of detecting seismic waves. Consequently, the surface $S_m(M_S)$ of Equation 2 is much larger than for a single-point observation because it includes the whole $\text{VOA}(\Delta\phi)$, and extends it in both latitude and longitude directions by $\Delta_m(M_S)$ degrees. When the surface of the VOA is non-zero, its surface is computed by the joint area

of two spherical caps for each surface wave magnitude (M_S) and each longitude separation ($\Delta\phi$) between the two spherical caps (i.e., the AEA and the IA). The average area over all possible $\Delta\phi$ values is then scaled to 4π as in Equation 2. The observation duration is reduced by the amount of time during which the VOA is zero.

Once these geometrical considerations have been taken into account, we still have to compute the maximum distance at which a quake can be observed by a point in the VOA defined by $\Delta_m(M_S)$.

For the 1.27 μm nighttime emissions, we need to convert the vertical particle velocity in the acoustic wave into airglow emission and compare this to the instrument noise. The vertical particle velocity at the altitude of the maximum emission rate of the 1.27 μm airglow ($z_{\text{IR1}} = 100 \text{ km}$) is provided by:

$$A_v(z_{\text{IR1}}) = \sqrt{\frac{\rho(0)c(0)}{\rho(z_{\text{IR1}})c(z_{\text{IR1}})}} \left(\frac{10^{-6}A_d(0)}{2\pi T_S} \right), \quad (10)$$

where $A_d(0)$ as function of surface wave magnitude is provided by inverting Equation 1. The sensitivity of 1.27 μm emissions is driven by the transport of the emitting molecules under the vertical velocity $A_v(z_{\text{IR1}})$ (Lognonné et al., 2016). The order of magnitude of this sensitivity is about 3.0%/m/s at 20 s period and 6%/m/s at 50 s period at 100 km altitude (Sutin et al., 2018). In addition, the estimated noise level of an imaging InfraRed (IR) camera targeting these emissions is about 0.5% of background emission level (Sutin et al., 2018).

For the 4.3 μm daytime emission, we focus on the 4.28 μm emission peak and assume that the emission altitude is approximately 135 km and that these emissions present a sensitivity of 1% per Kelvin variation of atmospheric temperature (López-Valverde et al., 2011). In order to convert the vertical particle velocity $A_v(z_{\text{IR2}})$ into temperature perturbation (in Kelvin), we use the impedance at $z_{\text{IR2}} = 135 \text{ km}$ altitude:

$$\begin{aligned} DP(z_{\text{IR2}}) &= \rho(z_{\text{IR2}})c(z_{\text{IR2}})A_v(z_{\text{IR2}}) \\ &= \rho(z_{\text{IR2}})c(z_{\text{IR2}}) \sqrt{\frac{\rho(0)c(0)}{\rho(z_{\text{IR2}})c(z_{\text{IR2}})}} \left(\frac{10^{-6}2\pi A_d(0)}{T_S} \right) \end{aligned} \quad (11)$$

which is similar to Equation 9 but at the altitude of the 4.28 μm emission peak. Then, we assume both the perfect gas law and the adiabatic nature of the acoustic wave perturbations in order to quantify the corresponding temperature changes through the following equation:

$$DT(z_{\text{IR2}}) = \frac{\gamma - 1}{\gamma} \frac{T(z_{\text{IR2}})}{P(z_{\text{IR2}})} DP(z_{\text{IR2}}), \quad (12)$$

where γ is the heat capacity ratio at altitude $z_{\text{IR2}} = 135 \text{ km}$, and $T(z_{\text{IR2}})$ and $P(z_{\text{IR2}})$ are the background temperature and pressure at this altitude, respectively. Finally, using the sensitivity of 1% per Kelvin of the 4.28 μm emission, we obtain the expected signal in percentage of background emission (López-Valverde et al., 2011). Concerning the instrument noise, we assume that the root-mean-square noise of the detector is about 0.125% of background emission (Sutin et al., 2018).

Gathering all these equations, we obtain the minimum number of events per year for a mission duration of 2 years, and for the two infrared emissions. This result is shown in Figure 5. The minimum surface wave magnitude that can be detected through these airglow emissions is around 5 for 4.3 μm emissions and around 6 for 1.27 μm emissions, but the required number of events per year is lower than 10. The minimum magnitude is the magnitude for which the signals on all the pixels is below the SNR limit, even if the quake is occurring within the VOA. These minimum surface wave magnitudes are consistent with the values provided by Sutin et al. (2018). At low magnitudes, we have a low variability of the minimum number of events per year because of the large extent of the observation area. Basically, when the event is above the minimum magnitude, it is detected as soon as it is inside the VOA, which is quite large. On the other hand, at large magnitudes all the events are detected, even if they are on the other side of the planet, and the number of detectable events (0.64 events per year) is directly linked to the observation duration of the AEA over the duration of the mission.

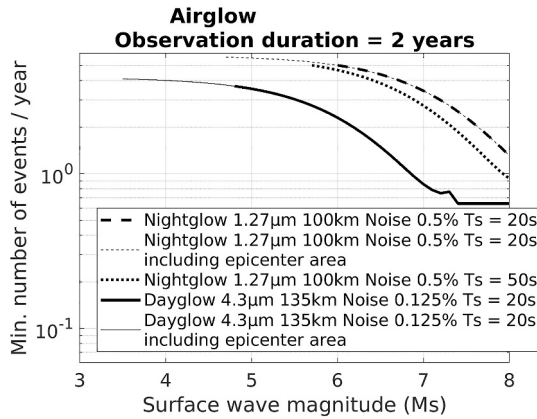


Figure 5. Minimum number of events per year as a function of surface wave magnitude required to measure at least one event of this magnitude during an airglow orbiter mission duration of 2 years. Results are provided for the two airglow emissions respectively at 1.27 μm (thick dashed line at 20 s period, thick dotted line at 50 s period) and at 4.28 μm (thick solid line). We also show the results for the 1.27 μm (thin dashed line) and the 4.28 μm (thin solid line) emissions at 20 s period but reducing the minimum distance between quake and sensor from 3° to 0.5° in order to include detections in the epicenter area.

From this figure, it is clear that the airglow emissions are best designed to detect quakes of surface wave magnitude larger than 5. This minimum magnitude cut-off can be decrease by 1.4 unit if signals within 300 km of the epicenter are considered, but this case is outside the scope of the assumptions used in this study. In addition, the capability of such observations to track surface wave propagation on the images is opening more opportunities to image lateral variations in the crust and the lithosphere. However, due to low-pass effects, induced by the vertical extent of airglow emission peaks and by the response of airglow emissions to acoustic forcing, these observations are probably limited to periods larger than 10 s (Lognonné et al., 2016; Sutin et al., 2018).

The balloon observations have a detection limit around 4.0–4.5 units of surface wave magnitude and can detect all quakes with surface wave magnitude larger than 7. In addition, they can detect higher frequency signals, with a useable bandwidth mainly for periods between 0.1 and 20 s. As for the airglow emissions, the lower bound of magnitude can be improved by 1.4 unit if signals close to the epicenter are considered. However, this observation

mean suffers for its single point measurement and from the short mission duration, estimated here to be 3 months. The balloon sensing is the method that would benefit the most from an increased observation time relative to the one used here.

Finally, for short duration deployment of a landed seismometer, the estimates present a large variability due to the large uncertainties on the final noise level of such an instrument. Assuming a noise level between 10^{-7} and 10^{-6} $\text{m/s}^2/\sqrt{\text{Hz}}$ at 20 s period, such an instrument can detect all quakes of surface wave magnitude larger than 5 to 6. In addition, for small quakes close to the sensor, the bandwidth of such an instrument would easily cover the 0.05–20 Hz range. However, such a concept is strongly limited by the short observation duration, assumed here to be 12 hr, such that it would allow us to investigate only seismic events that are occurring more than 800 times per Earth year.

2.4.6. Comparing the Different Seismic Wave Measurements Concepts

As already done for the balloon detection estimates, we also provide estimates for a minimum distance of detection reduced to 0.5° in order to include the detection of seismic waves close to the epicenter area. As observed for the balloon estimates, including this area is lowering the minimum surface wave magnitude by 1.4. However, in this close range, Equation 1 is no longer valid. In addition, the detection of such signals based on only a few pixels of the camera image is not ensuring that these signals can be deciphered from background noise variations. This is why we remain conservative by presenting only the results for a minimum distance of 3°.

It should be noted that airglow images can potentially provide ways to detect signals below a SNR of 3 by data processing methods exploiting the redundant information brought by consecutive images (Sutin et al., 2018).

Figure 6 assembles the detection capabilities of a landed seismometer, balloon-based microbarometer, and an orbiter-based airglow detector. The ground-based DAS and rotation detection concepts are not included because the technology is currently infeasible. For ground strain sensing, DAS systems suffers from lack of control over the cable's layout. For seismic ground rotation sensing, there are currently no instruments available with low enough intrinsic noise.

It should be noted that the effect of mission duration extension on these minimum number of events per year estimates is easy to handle. If you multiply the observation duration by X, you must divide the minimum number of events per year by X for all magnitudes. This simple relation

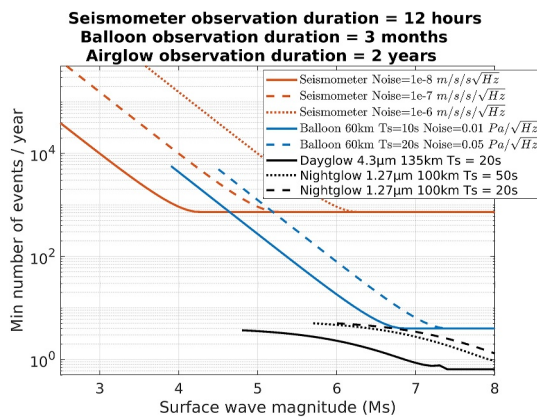


Figure 6. Minimum number of events per year as a function of surface wave magnitude required to measure at least one event of this magnitude for all the detection methods. Landed seismometers in brown, balloon estimates in blue, and airglow emissions in black.

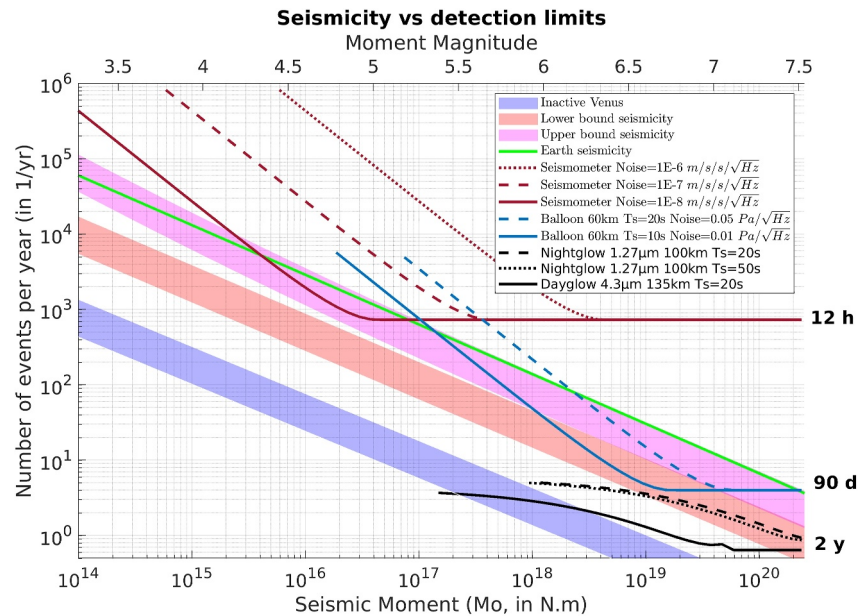


Figure 7. Minimum number of events per year as a function of seismic moment (in N.m) on the bottom and moment magnitude on top required to measure at least one event of this magnitude for all the detection methods (lines) compared to end-member Venus seismicity estimates (shaded areas) by van Zelst et al. (2024): an inactive Venus (blue), lower bound active Venus (red) and upper bound active Venus (magenta). For comparison, Earth's seismicity is also provided as a thick light green line. Balloon estimates are in dark blue, landed seismometers in brown, and airglow emissions in black. Constant estimate at large magnitude are limited by observation duration indicated on the left of the figure.

allows the reader to translate these estimates to any observation duration. The effect of increasing the noise level by a factor X is also simple to quantify: it corresponds to a shift of the curves to the right by $\log_{10}(X)$ units of magnitude.

3. Comparing of Detection Capabilities With Current Seismicity Estimates

Our estimates of detection capabilities are shown in Figure 6 as a function of surface wave magnitude M_S which was defined following the IASPEI standard and corresponds to the definition of M_S_{20} by (Bormann et al., 2013). However, seismicity estimates are usually provided as a function of seismic moment magnitude M_W which is a better representation of the quake physics. In order to convert from M_S to M_W , we use the following relation defined by Bormann et al. (2013) for quake moment magnitudes smaller than 6.8 that are of our main interest:

$$M_W = 0.667 M_S + 2.18. \quad (13)$$

The error bar in this conversion is on the order of 0.3 magnitude unit, but even such large errors could in fact be smaller than the error we may have due to the unknown internal structure of Venus. Eventually, the moment magnitude is converted to the seismic moment M_0 (in Nm) by the standard conversion formula $M_W = \frac{2}{3}(\log_{10}(M_0) - 9.1)$.

Once M_S has been converted into M_W or M_0 , we can directly compare our detection limits of at least one quake with a signal-to-noise ratio larger than three over the mission duration with the recent Venus seismicity estimates by van Zelst et al. (2024). They estimated upper and lower bounds on the expected annual seismicity of Venus by scaling the seismicity of the Earth. For different tectonic settings on Venus, they assumed different Earth analogs and took into account the lower seismogenic zone thickness of Venus. van Zelst et al. (2024) presented three end-member estimates: an “inactive” Venus, where the planet exhibits a global background seismicity rate analogous to that of continental intraplate settings on Earth, resulting in a few hundred quakes $\geq M_w 4$ per year; and two active scenarios where it is assumed that the coronae, fold belts, and rifts of Venus are currently seismically active. As a realistic lower bound of a seismically active Venus, they find 1,161–3,609 venusquakes $\geq M_w 4$ annually and 5,715–17,773 venusquakes $\geq M_w 4$ per year as a maximum upper bound for an active Venus. This latter upper

figure is similar to the amount of seismicity on Earth, although generally the estimates of Venus' expected seismicity are lower than that of Earth. The comparison of our detection limits with van Zelst et al. (2024)'s estimates is presented in Figure 7.

The detection limits presented here should be taken with caution for two main reasons. First, the limitations presented in the next section induce an error bar on the order of one order of magnitude on these estimates. Secondly, we investigated mainly seismic signals around the 20 s period whereas the expected bandwidths of the different methods are different with an upper bound frequency of 10 Hz for ground and balloon sensors to 0.1 Hz for airglow observations. However, if the reader wants to scale these curves to a different observation duration, this is straightforward to perform, because multiplying the observation duration by X is simply the same as dividing the minimum number of events per year by X , for all magnitudes.

Despite these limitations, some interesting observations can be made in Figure 7. The ground-based sensors can be considered adequate for seismic wave detection if their noise level at 20 s period is below $10^{-8} \text{ m/s}^2/\sqrt{\text{Hz}}$ and if they are deployed in an active seismic area that would allow us to detect quakes of magnitudes smaller than 4.0. The pressure sensors on balloon platforms allow for probing quake magnitudes in the 5.0 to 7.0 moment magnitude range and mainly for seismic signal frequencies in the 0.05–10 Hz range. The airglow measurements have the lowest detection limits due to the low noise level and the long duration of the observations. In addition, the output movie of wave propagation would allow for determining the source location and investigating variations in seismic surface speeds over the planet that could be related to lateral heterogeneities in the shallow seismic wave structure of the crust. However, this measurement concept is limited to seismic moment magnitudes larger than 5.5 and to wave periods larger than 5 s.

Eventually, it is interesting to note that airglow and balloon measurements are very complementary because they cover different frequency ranges, different locations and provide different information on the seismic wavefield. The same quake could be observed with a good probability by both balloon and airglow methods if the balloon observation duration is increased up to one or 2 year for quake moment magnitudes larger than 6.0. This double observation would drastically reduce the probability of misinterpretation with an atmospheric perturbation, and it would provide the seismic source frequency cut-off from balloon observation as well as the lateral variations of seismic surface wave velocity from airglow imager data.

4. Limitations

Our analysis was performed under certain assumptions that leave room for future improvements and exploration.

First, the spatial dependence of seismicity estimates is not taken into account in our estimates of quake detectability, despite the likelihood that certain areas on Venus exhibit higher seismic activity compared to others. Even if this issue is not so critical for airglow measurements that will cover a large part of the planet surface, it is obvious that ground sensor deployments should target the most active regions in order to improve their detection capabilities. The balloon missions are also expected to cover more equatorial regions than polar regions due to deployment and mission duration constraints.

A second important limitation is the uncertainty in the noise levels of each measurement concept. Even though we consider reasonable assumptions on these numbers and provided estimates for different noise levels, detailed noise models of these measurement concepts are required to fully validate our analysis. Mimoun et al. (2017) provides an example of a detailed noise model for a seismometer instrument. An inherent difficulty to the noise model exercise is that the mission parameters (lander size, instrument performance parameters, etc.) must be known in order for the analysis to be valid.

Moreover, the method used to relate ground movements to quake magnitude and the frequencies considered here (periods between 10 and 50 s) are mainly relevant for quake moment magnitudes between 4.0 and 6.8 (Bormann et al., 2013). For quake moment magnitudes smaller than 4.0, other methods and frequency ranges should be considered.

Lastly, our assumptions are valid mainly for quakes at distances larger than 300 km from the sensor. The case of quakes at closer distances has been partly investigated for balloon and airglow measurements, but not reported in the final estimates. These strong signals close to the source are decreasing by 1.4 unit the minimum detection magnitude, at the expense of making their identification and interpretation more complex.

5. Conclusion

Our study provides a first estimate of the detection capabilities of long period seismic surface waves on Venus by various measurement concepts: ground sensors including seismometers, DAS, and rotation sensors; infrasound sensors on balloons; and airglow imagers onboard orbiters. We also compare these estimates with recent predictions of Venus seismicity. The airglow measurement concept appears to be most relevant in light of the current estimates of seismicity, but it is limited to moment magnitudes larger than 5.5 and wave periods larger than 5 s. We find that a minimum measurement duration of 2 years ensures a good probability to detect large magnitude quakes for airglow measurements. Infrasound sensors onboard balloons must ensure an overall noise level below $10^{-2} \text{ Pa}/\sqrt{\text{Hz}}$ at 10 s period and a measurement duration larger than 3 months to obtain a good probability of quake detection. The ground sensors are strongly limited by their measurement duration but also by their noise, mainly due to instrument self-noise for potential ground rotation sensors, and noise induced by the installation or environment for seismometers and potential DAS fiber measurements that would be effective only with an overall acceleration noise level at 20 s period below $10^{-8} \text{ m/s}^2/\sqrt{\text{Hz}}$. Uncertainties ranging up to one order of magnitude impact these detection limit estimates due to limitations that could be improved in various directions by future studies. Potential directions of improvement would be to take into account the geographical distribution of quakes, a full modeling of the amplitude of seismic and infrasound waves, detailed noise models of the measurement concepts, and the analysis of the science case of a detection close to the epicenter. Rather than definitively concluding on one measurement concept, our study allows us to enhance the advantages and limitations of each measurement concept. Our estimates of detection capabilities can also be used to drive requirements on future mission concepts. As an example, balloon missions should ensure measurements at altitudes where the atmosphere is stable and quiet in order to ensure a proper background noise level, and these missions would benefit of extending their duration to 6 months or 1 year to ensure the detection of large magnitude quakes. The long duration balloon measurements and the airglow imagers appear to be very complementary because they have a good probability to detect the same quake for moment magnitudes larger than 6.0, and would thus provide different information on the seismic wavefield in different frequency ranges.

Despite the recent selection of various space missions to Venus, none of these will target the detection and characterization of seismic waves to investigate Venus' internal structure in better detail. The most realistic programmatic scenario for the implementation of any of the measurement concepts described in this study in the next decade is probably the deployment of such concepts by a small satellite as a piggyback payload on one of these missions. In the longer term, larger missions would benefit from combining balloon and airglow measurement concepts if the balloon mission duration can be extended above 3 months.

Data Availability Statement

All the codes and input data used to create the figures in this article are available at the following zenodo repository <https://zenodo.org/records/13134375> (Garcia, 2024).

References

- Avduevskii, V. S., Vishnevetskii, S. L., Golov, I. A., Karpeiskii, I. I., Lavrov, A. D., Likhushin, V. I., et al. (1977). Measurement of wind velocity on the surface of Venus during the operation of stations Venera 9 and Venera 10. *Cosmic Research*, *14*(5), 710–713.
- Banfield, D., Spiga, A., Newman, C., Forget, F., Lemmon, M., Lorenz, R., et al. (2020). The atmosphere of Mars as observed by InSight. *Nature Geoscience*, *13*(3), 190–198. <https://doi.org/10.1038/s41561-020-0534-0>
- Bass, H. E., & Chambers, J. P. (2001). Absorption of sound in the Martian atmosphere. *Acoustical Society of America Journal*, *109*(5), 2371. <https://doi.org/10.1121/1.4744345>
- Beauchamp, P., Gilmore, M. S., Lynch, R. J., Sarli, B. V., Nicoletti, A., Jones, A., et al. (2021). Venus flagship mission concept: A decadal survey study. In *2021 IEEE aerospace conference (50100)* (pp. 1–18).
- Bernauer, F., Behnen, K., Wassermann, J., Egdorf, S., Igel, H., Donner, S., et al. (2021). Rotation, strain, and translation sensors performance tests with active seismic sources. *Sensors*, *21*(1), 264. <https://doi.org/10.3390/s21010264>
- Bernauer, F., Garcia, R. F., Murdoch, N., Dehant, V., Sollberger, D., Schmelzbach, C., et al. (2020a). Exploring planets and asteroids with 6DoF sensors: Utopia and realism. *Earth Planets and Space*, *72*(1), 191. <https://doi.org/10.1186/s40623-020-01333-9>
- Bernauer, F., Wassermann, J., & Igel, H. (2020b). Dynamic tilt correction using direct rotational motion measurements. *Seismological Research Letters*, *91*(5), 2872–2880. <https://doi.org/10.1785/0220200132>
- Bormann, P. (2002). New manual of seismological observatory practice. *GeoForschungsZentrum*. https://doi.org/10.2312/GFZ.NMSOP-2_ch4
- Bormann, P., & Dewey, J. W. (2012). The new IASPEI standards for determining magnitudes from digital data and their relation to classical magnitudes.
- Bormann, P., Wendt, S., & DiGiacomo, D. (2013). Seismic sources and source parameters. In *New manual of seismological observatory practice* (Vol. 2(NMSOP2), pp. 1–259). Deutsches GeoForschungsZentrum GFZ. https://doi.org/10.2312/GFZ.NMSOP-2_ch3

Acknowledgments

We thank an anonymous reviewer and Jim Cutts for improving this study in different directions. We thank Lauriane Soret for allowing us to reproduce part of her work in Figure 4(a). This research was supported by the International Space Science Institute (ISSI) in Bern, Switzerland through International Team project #566: “Seismicity on Venus: Prediction & Detection”, led by Iris van Zelst. RFG acknowledges funding by CNES through APR project “VenusGeox”. IvZ, JM, and ACP acknowledge the financial support and endorsement from the DLR Management Board Young Research Group Leader Program and the Executive Board Member for Space Research and Technology. IvZ also gratefully acknowledges the support by the Deutsche Forschungsgemeinschaft (DFG, German Research Foundation), Project-ID 263649064—TRR 170. SPN, CMS, and QB acknowledge support from the Research Council of Norway basic research program FRIPRO through the project “Airborne inversion of Rayleigh waves” under Contract 335903. ML acknowledges funding from the European Union's Horizon Europe research and innovation program under the Marie Skłodowska-Curie Grant agreement 101110489/MuSICA-V. AG acknowledges support by the Swiss National Science Foundation Postdoc Mobility Grant P500PN_21729 and AG and MPP were supported by the Jet Propulsion Laboratory, California Institute of Technology, under contract (80NM0018D0004) with the National Aeronautics and Space Administration. A. H. is funded by the UK Space Agency under Grant numbers ST/W002523/1, ST/W002949/1 and ST/Y005597/1.

- Brissaud, Q., Krishnamoorthy, S., Jackson, J. M., Bowman, D. C., Komjathy, A., Cutts, J. A., et al. (2021). The first detection of an earthquake from a balloon using its acoustic signature. *Geophysical Research Letters*, *48*(12). <https://doi.org/10.1029/2021gl093013>
- Byrne, P. K., Ghail, R. C., Şengör, A. M. C., James, P. B., Klimczak, C., & Solomon, S. C. (2021). A globally fragmented and mobile lithosphere on Venus. *Proceedings of the National Academy of Sciences*, *118*(26), e2025919118. <https://doi.org/10.1073/pnas.2025919118>
- Carrasco, S., Knapmeyer-Endrun, B., Margerin, L., Xu, Z., Joshi, R., Schimmel, M., et al. (2023). Constraints for the Martian crustal structure from Rayleigh waves ellipticity of large seismic events. *Geophysical Research Letters*, *50*(16), e2023GL104816. <https://doi.org/10.1029/2023GL104816>
- Chan, H. M., Parker, A. R., Piazza, A., & Richards, W. L. (2015). Fiber-optic sensing system: Overview, development and deployment in flight at NASA. In *2015 IEEE avionics and vehicle fiber-optics and photonics conference (AVFOP)* (pp. 71–73).
- Chen, L., Neudeck, P. G., Meredith, R. D., Lukco, D., Spry, D. J., Nakley, L. M., et al. (2019). Sixty earth-day test of a prototype Pt/HTCC alumina package in a simulated Venus environment. *Journal of Microelectronics and Electronic Packaging*, *16*(2), 78–83. <https://doi.org/10.4071/imaps.873073>
- Cheng, F., Chi, B., Lindsey, N. J., Dawe, T. C., & Ajo-Franklin, J. B. (2021). Utilizing distributed acoustic sensing and ocean bottom fiber optic cables for submarine structural characterization. *Scientific Reports*, *11*(1), 5613. <https://doi.org/10.1038/s41598-021-84845-y>
- Daley, T., Miller, D., Dodds, K., Cook, P., & Freifeld, B. (2016). Field testing of modular borehole monitoring with simultaneous distributed acoustic sensing and geophone vertical seismic profiles at Citronelle, Alabama. *Geophysical Prospecting*, *64*(5), 1318–1334. <https://doi.org/10.1111/1365-2478.12324>
- Drilleau, M., Samuel, H., Garcia, R. F., Rivoldini, A., Perrin, C., Michaut, C., et al. (2022). Marsquake locations and 1-D seismic models for Mars from InSight data. *Journal of Geophysical Research (Planets)*, *127*(9), e07067. <https://doi.org/10.1029/2021JE007067>
- Dumoulin, C., Tobie, G., Verhoeven, O., Rosenblatt, P., & Rambaux, N. (2017). Tidal constraints on the interior of Venus. *Journal of Geophysical Research (Planets)*, *122*(6), 1338–1352. <https://doi.org/10.1002/2016JE005249>
- Durán, C., Khan, A., Ceylan, S., Charalambous, C., Kim, D., Drilleau, M., et al. (2022a). Observation of a core-diffracted P-wave from a farside impact with implications for the lower-mantle structure of Mars. *Geophysical Research Letters*, *49*(21), e2022GL100887. <https://doi.org/10.1029/2022GL100887>
- Durán, C., Khan, A., Ceylan, S., Zenhäuser, G., Stähler, S., Clinton, J. F., & Giardini, D. (2022b). Seismology on Mars: An analysis of direct, reflected, and converted seismic body waves with implications for interior structure. *Physics of the Earth and Planetary Interiors*, *325*, 106851. <https://doi.org/10.1016/j.pepi.2022.106851>
- Garcia, R. F. (2024). Input data, codes, figures and numeric data used in the figures of the paper entitled “Seismic wave detectability on Venus using ground deformation sensors, infrasound sensors on balloons and airglow imagers” by Garcia et al. [Dataset]. <https://doi.org/10.5281/zenodo.13134375>
- Garcia, R. F., Brissaud, Q., Rolland, L., Martin, R., Komatitsch, D., Spiga, A., et al. (2017). Finite-difference modeling of acoustic and gravity wave propagation in Mars atmosphere: Application to infrasounds emitted by meteor impacts. *Space Science Reviews*, *211*(1–4), 547–570. <https://doi.org/10.1007/s11214-016-0324-6>
- Garcia, R. F., Drossart, P., Piccioni, G., López-Valverde, M., & Occhipinti, G. (2009). Gravity waves in the upper atmosphere of Venus revealed by CO₂ nonlocal thermodynamic equilibrium emissions. *Journal of Geophysical Research (Planets)*, *114*(E5), E00B32. <https://doi.org/10.1029/2008JE003073>
- Garcia, R. F., Klotz, A., Hertzog, A., Martin, R., Gérier, S., Kassarian, E., et al. (2022). Infrasound from large earthquakes recorded on a network of balloons in the stratosphere. *Geophysical Research Letters*, *49*(15). <https://doi.org/10.1029/2022gl098844>
- Garcia, R. F., Lognonné, P. H., & Bonnin, X. (2005). Detecting atmospheric perturbations produced by Venus quakes. *Geophysical Research Letters*, *32*(16), 1–4. <https://doi.org/10.1029/2005GL023558>
- Garvin, J. B., Getty, S. A., Arney, G. N., Johnson, N. M., Kohler, E., Schwer, K. O., et al. (2022). Revealing the mysteries of Venus: The DAVINCI mission. *The Planetary Science Journal*, *3*(5), 117. <https://doi.org/10.3847/psj/ac63c2>
- Gérard, J. C., Sağlam, A., Piccioni, G., Drossart, P., Cox, C., Erard, S., et al. (2008). Distribution of the O₂ infrared nightglow observed with VIRTIS on board Venus Express. *Geophysical Research Letters*, *35*(2), L02207. <https://doi.org/10.1029/2007GL032021>
- Gérard, J. C., Soret, L., Piccioni, G., & Drossart, P. (2014). Latitudinal structure of the Venus O₂ infrared airglow: A signature of small-scale dynamical processes in the upper atmosphere. *Icarus*, *236*, 92–103. <https://doi.org/10.1016/j.icarus.2014.03.028>
- Gerier, S., Garcia, R. F., Martin, R., & Hertzog, A. (2024). Forward modeling of quake’s infrasound recorded in the stratosphere on board balloon platforms. *Earth Planets and Space*, *76*(1), 1–20. <https://doi.org/10.1186/s40623-024-02030-7>
- Gilli, G., Lebonnois, S., González-Galindo, F., López-Valverde, M. A., Stolzenbach, A., Lefèvre, F., et al. (2017). Thermal structure of the upper atmosphere of Venus simulated by a ground-to-thermosphere GCM. *Icarus*, *281*, 55–72. <https://doi.org/10.1016/j.icarus.2016.09.016>
- Gilli, G., Navarro, T., Lebonnois, S., Quirino, D., Silva, V., Stolzenbach, A., et al. (2021). Venus upper atmosphere revealed by a GCM: II. Model validation with temperature and density measurements. *Icarus*, *366*, 114432. <https://doi.org/10.1016/j.icarus.2021.114432>
- Glass, D. E., Jones, J.-P., Shevade, A. V., Bhakta, D., Raub, E., Sim, R., & Bugga, R. V. (2020). High temperature primary battery for Venus surface missions. *Journal of Power Sources*, *449*, 227492. <https://doi.org/10.1016/j.jpowsour.2019.227492>
- Gudkova, T. V., & Zharkov, V. N. (2020). Models of the internal structure of the Earth-like Venus. *Solar System Research*, *54*(1), 20–27. <https://doi.org/10.1134/S0038094620010049>
- Gülcher, A. J. P., Gerya, T. V., Montési, L. G. J., & Munch, J. (2020). Corona structures driven by plume–lithosphere interactions and evidence for ongoing plume activity on Venus. *Nature Geoscience*, *13*(8), 547–554. <https://doi.org/10.1038/s41561-020-0606-1>
- Heracle. (2023). Step index multimode fibers metal coated series: Gold. Retrieved from <https://www.heracle.de/products/step-index-multimode-fibers-metal-coated-series-gold/?lang=en>
- Herrick, R., & Hensley, S. (2023). Surface changes observed on a Venesian volcano during the Magellan mission. *Science*, *379*(6638), 1205–1208. <https://doi.org/10.1126/science.abm7735>
- Hudson, T. S., Baird, A. F., Kendall, J.-M., Kufner, S.-K., Brisbourne, A. M., Smith, A. M., et al. (2021). Distributed acoustic sensing (DAS) for natural microseismicity studies: A case study from Antarctica. *Journal of Geophysical Research: Solid Earth*, *126*(7), e2020JB021493. <https://doi.org/10.1029/2020jb021493>
- Hunter, G., Kremic, T., & Neudeck, P. G. (2021). High temperature electronics for Venus surface applications: A summary of recent technical advances. *Bulletin of the American Astronomical Society*, *53*(4), 399. <https://doi.org/10.3847/25c2cf6e.e3883e19>
- Jacobsen, W., Soufiane, A., & D’Urso, J. (2018). 500°C-rated optical fibers for high temperature applications. *80th EAGE Conference and Exhibition, 2018*, 1–5.
- Joussot, P., Currenti, G., Schwarz, B., Chalari, A., Tilmann, F., Reinsch, T., et al. (2022). Fibre optic distributed acoustic sensing of volcanic events. *Nature Communications*, *13*(1), 1753. <https://doi.org/10.1038/s41467-022-29184-w>

- Kerzhanovich, V. V., & Marov, M. I. (1983). The atmospheric dynamics of Venus according to Doppler measurements by the Venera entry probes. In *Venus* (pp. 766–778). The University of Arizona Press.
- Kim, D., Banerdt, W. B., Ceylan, S., Giardini, D., Lekić, V., Lognonné, P., et al. (2022). Surface waves and crustal structure on Mars. *Science*, 378(6618), 417–421. <https://doi.org/10.1126/science.abq7157>
- Klaasen, S., Paitz, P., Lindner, N., Dettmer, J., & Fichtner, A. (2021). Distributed acoustic sensing in volcano-glacial environments—Mount Meager, British Columbia. *Journal of Geophysical Research: Solid Earth*, 126(11), e2021JB022358. <https://doi.org/10.1029/2021JB022358>
- Klaasen, S., Thrastarson, S., Çubuk-Sabuncu, Y., Jónsdóttir, K., Gebraad, L., Paitz, P., & Fichtner, A. (2023). Subglacial volcano monitoring with fibre-optic sensing: Grímsvötn, Iceland. *Volcanica*, 6(2), 301–311. <https://doi.org/10.30909/vol.06.02.301311>
- Kremic, T., Ghail, R., Gilmore, M., Hunter, G., Kiefer, W., Limaye, S., et al. (2020). Long-duration Venus lander for seismic and atmospheric science. *Planetary and Space Science*, 190, 104961. <https://doi.org/10.1016/j.pss.2020.104961>
- Kremnev, R. S., Linkin, V. M., Lipatov, A. N., Pichkadze, K. M., Shurupov, A. A., Terterashvili, A. V., et al. (1986). VEGA balloon system and instrumentation. *Science*, 231(4744), 1408–1411. <https://doi.org/10.1126/science.231.4744.1408>
- Krishnamoorthy, S., & Bowman, D. C. (2023). A “floatilla” of airborne seismometers for Venus. *Geophysical Research Letters*, 50(2), e2022GL100978. <https://doi.org/10.1029/2022GL100978>
- Krishnamoorthy, S., Bowman, D. C., Hough, E., Yap, Z., G erier, S., Wilding, J., et al. (2023). Progress towards balloon-based seismic studies on Venus. *AGU fall meeting abstracts, 2023*, P31F–P3147.
- Ksanfomaliti, L. V., Goroshkova, N. V., & Khondyrev, V. K. (1983). Wind velocity on the Venus surface from acoustic measurements. *Kosmicheskie Issledovaniia*, 21, 218–224.
- Ksanfomaliti, L. V., Zubkova, V. M., Morozov, N. A., & Petrova, N. A. (1982). Microseisms at the Venera 13 and Venera 14 landing sites. *Pis'ma v Astronomicheskii Zhurnal*, 8, 444–447.
- Lebonnois, S., Schubert, G., Forget, F., & Spiga, A. (2018). Planetary boundary layer and slope winds on Venus. *Icarus*, 314, 149–158. <https://doi.org/10.1016/j.icarus.2018.06.006>
- Lef evre, M. (2022). Venus boundary layer dynamics: Eolian transport and convective vortex. *Icarus*, 387, 115167. <https://doi.org/10.1016/j.icarus.2022.115167>
- Lef evre, M., Spiga, A., Lebonnois, S., & Forget, F. (2024). Venus near-surface dynamics: Slope winds and dust transport. In *Europlanet science congress 2024 abstracts*. <https://doi.org/10.5194/eps2024-384>
- Lindsey, N. J., & Martin, E. R. (2021). Fiber-optic seismology. *Annual Review of Earth and Planetary Sciences*, 49(1), 309–336. <https://doi.org/10.1146/annurev-earth-072420-065213>
- Lior, I., Sladen, A., Rivet, D., Ampuero, J.-P., Hello, Y., Becerril, C., et al. (2021). On the detection capabilities of underwater distributed acoustic sensing. *Journal of Geophysical Research: Solid Earth*, 126(3), e2020JB020925. <https://doi.org/10.1029/2020jb020925>
- Lognonn e, P., Banerdt, W. B., Clinton, J., Garcia, R. F., Giardini, D., Knapmeyer-Endrun, B., et al. (2023). Mars seismology. *Annual Review of Earth and Planetary Sciences*, 51(1), 643–670. <https://doi.org/10.1146/annurev-earth-031621-073318>
- Lognonn e, P., Banerdt, W. B., Giardini, D., Pike, W. T., Christensen, U., Laudet, P., et al. (2019). SEIS: Insight’s seismic experiment for internal structure of Mars. *Space Science Reviews*, 215(1), 12. <https://doi.org/10.1007/s11214-018-0574-6>
- Lognonn e, P., Karakostas, F., Rolland, L., & Nishikawa, Y. (2016). Modeling of atmospheric-coupled Rayleigh waves on planets with atmosphere: From Earth observation to Mars and Venus perspectives. *Journal of the Acoustical Society of America*, 140(2), 1447–1468. <https://doi.org/10.1121/1.4960788>
- L opez-Valverde, M. A., L opez-Puertas, M., Funke, B., Gilli, G., Garcia-Comas, M., Drossart, P., et al. (2011). Modeling the atmospheric limb emission of CO₂ at 4.3 μm in the terrestrial planets. *Planetary and Space Science*, 59(10), 988–998. <https://doi.org/10.1016/j.pss.2010.02.001>
- Lorenz, R. D. (2012). Planetary seismology—Expectations for lander and wind noise with application to Venus. *Planetary and Space Science*, 62(1), 86–96. <https://doi.org/10.1016/j.pss.2011.12.010>
- Lorenz, R. D. (2016). Surface winds on Venus: Probability distribution from in-situ measurements. *Icarus*, 264, 311–315. <https://doi.org/10.1016/j.icarus.2015.09.036>
- Lorenz, R. D., & Panning, M. P. (2018). Empirical recurrence rates for ground motion signals on planetary surfaces. *Icarus*, 303, 273–279. <https://doi.org/10.1016/j.icarus.2017.10.008>
- Makela, J. J., Lognonn e, P., H ebert, H., Gehrels, T., Rolland, L., Allgeyer, S., et al. (2011). Imaging and modeling the ionospheric airglow response over Hawaii to the tsunami generated by the Tohoku earthquake of 11 March 2011. *Geophysical Research Letters*, 38(13), L00G02. <https://doi.org/10.1029/2011GL047860>
- Margot, J.-L., Campbell, D. B., Giorgini, J. D., Jao, J. S., Snedeker, L. G., Ghigo, F. D., & Bonsall, A. (2021). Spin state and moment of inertia of Venus. *Nature Astronomy*, 5(7), 676–683. <https://doi.org/10.1038/s41550-021-01339-7>
- Martinez, A., Lebonnois, S., Millour, E., Pierron, T., Moisan, E., Gilli, G., & Lef evre, F. (2023). Exploring the variability of the Venusian thermosphere with the IPSL Venus GCM. *Icarus*, 389, 115272. <https://doi.org/10.1016/j.icarus.2022.115272>
- Mimoun, D., Murdoch, N., Lognonn e, P., Hurst, K., Pike, W. T., Hurley, J., et al. (2017). The noise model of the InSight seismometer of the InSight mission to Mars. *Space Science Reviews*, 211(1–4), 383–428. <https://doi.org/10.1007/s11214-017-0409-x>
- Moroz, V. I. (1983). Summary of preliminary results of the Venera 13 and Venera 14 missions. In *Venus* (pp. 45–68). The University of Arizona Press.
- Nachman, A. I., Smith, J. F. III, & Waag, R. C. (1990). An equation for acoustic propagation in inhomogeneous media with relaxation losses. *Journal of the Acoustical Society of America*, 88(3), 1584–1595. <https://doi.org/10.1121/1.400317>
- N asholm, S. P., Iranpour, K., Wuestefeld, A., Dando, B. D., Baird, A. F., & Oye, V. (2022). Array signal processing on distributed acoustic sensing data: Directivity effects in slowness space. *Journal of Geophysical Research: Solid Earth*, 127(2), e2021JB023587. <https://doi.org/10.1029/2021JB023587>
- Neudeck, P. G., Spry, D. J., Krasowski, M. J., Prokop, N. F., Beheim, G. M., Chen, L.-Y., & Chang, C. W. (2018). Year-long 500°C operational demonstration of up-scaled 4H-SiC JFET integrated circuits. *Journal of Microelectronics and Electronic Packaging*, 15(4), 163–170. <https://doi.org/10.4071/imeps.729648>
- Noe, S., Yuan, S., Montagner, J. P., & Igel, H. (2022). Anisotropic elastic parameter estimation from multicomponent ground-motion observations: A theoretical study. *Geophysical Journal International*, 229(2), 1462–1473. <https://doi.org/10.1093/gji/ggac006>
- Ochchipinti, G., Coisson, P., Makela, J. J., Allgeyer, S., Kherani, A., Hebert, H., & Lognonn e, P. (2011). Three-dimensional numerical modeling of tsunami-related internal gravity waves in the Hawaiian atmosphere. *Earth Planets and Space*, 63(7), 847–851. <https://doi.org/10.5047/eps.2011.06.051>
- O’Rourke, J. G. (2021). ADVENTS: Assessment and discovery of Venus’ past evolution and near-term climatic and geophysical state. In *Mission concept study report to the NRC planetary science and astrobiology decadal survey 2023–2032*. NASA Goddard Space Flight Center, Green Bank. Retrieved from <https://smd-cms.nasa.gov/wp-content/uploads/2023/10/advents-venus-orbiter-aerobot-and-dropsonde.pdf>

- Parker, A. R., Chan, H. M., Lopez-Zepeda, J., & Schallhorn, P. A. (2024). Design, fabrication, testing and validation of a ruggedized fiber optics sensing system (FOSS) for launch application. In *AIAA SCITECH 2024 forum*. <https://doi.org/10.2514/6.2024-2268>.2268
- Petculescu, A. (2016). Acoustic properties in the low and middle atmospheres of Mars and Venus. *Journal of the Acoustical Society of America*, *140*(2), 1439–1446. <https://doi.org/10.1121/1.4960784>
- Peterson, J. (1993). *Observation and modeling of background seismic noise* (pp. 92–322). U.S. Geol. Surv. Open-File Rept.
- Pinot, B., Mimoun, D., Murdoch, N., Onodera, K., Johnson, C., Mittelholz, A., et al. (2024). The in situ evaluation of the SEIS noise model. *Space Science Reviews*, *220*(3), 26. <https://doi.org/10.1007/s11214-024-01056-3>
- Reinsch, T., & Henniges, J. (2010). Temperature-dependent characterization of optical fibres for distributed temperature sensing in hot geothermal wells. *Measurement Science and Technology*, *21*(9), 094022. <https://doi.org/10.1088/0957-0233/21/9/094022>
- Sagdeev, R. Z. (1986). An overview of the Soviet VEGA balloon experiment and studies of the atmosphere of Venus. An overview of the Soviet Vega balloon experiment and studies of the atmosphere of Venus *Transl. into English Pisma v Astronomicheskii Zhurnal (Moscow, USSR)*, *12*(1), 5–95.
- Sagdeev, R. Z., Linkin, V. M., Kerzhanovich, V. V., Lipatov, A. N., Shurupov, A. A., Blamont, J. E., et al. (1986a). Overview of VEGA Venus balloon in situ meteorological measurements. *Science*, *231*(4744), 1411–1414. <https://doi.org/10.1126/science.231.4744.1411>
- Sagdeev, R. Z., Linkin, V. M., Lipatov, A. N., Pichkadze, K. M., Shurupov, A. A., Terterashvili, A. V., et al. (1986b). The VEGA Venus balloon experiment. *Science*, *231*(4744), 1408–1411. <https://doi.org/10.1126/science.231.4744.1408>
- Samuel, H., Drilleau, M., Rivoldini, A., Xu, Z., Huang, Q., Garcia, R. F., et al. (2023). Geophysical evidence for an enriched molten silicate layer above Mars's core. *Nature*, *622*(7984), 712–717. <https://doi.org/10.1038/s41586-023-06601-8>
- Schmelzbach, C., Donner, S., Igel, H., Sollberger, D., Taufiqurrahman, T., Bernauer, F., et al. (2018). Advances in 6C seismology: Applications of combined translational and rotational motion measurements in global and exploration seismology. *Geophysics*, *83*(3), WC53–WC69. <https://doi.org/10.1190/geo2017-0492.1>
- Seiff, A., & Kirk, D. B. (1991). Waves in Venus' middle and upper atmosphere; Implication of Pioneer Venus probe data above the clouds. *Journal of Geophysical Research*, *96*(A7), 11021–11032. <https://doi.org/10.1029/91JA01101>
- Smrekar, S., Hensley, S., Nybakken, R., Wallace, M., Perkovic-Martin, D., You, T.-H., et al. (2022). VERITAS (Venus emissivity, radio science, InSAR, topography, and spectroscopy): A discovery mission. In *2022 IEEE aerospace conference (AERO)*. IEEE. <https://doi.org/10.1109/aero53065.2022.9843269>
- Smrekar, S. E., Ostberg, C., & O'Rourke, J. G. (2023). Earth-like lithospheric thickness and heat flow on Venus consistent with active rifting. *Nature Geoscience*, *16*(1), 13–18. <https://doi.org/10.1038/s41561-022-01068-0>
- Smrekar, S. E., Stofan, E. R., Mueller, N., Treiman, A., Elkins-Tanton, L., Helbert, J., et al. (2010). Recent hotspot volcanism on Venus from VIRTIS emissivity data. *Science*, *328*(5978), 605–608. <https://doi.org/10.1126/science.1186785>
- Sollberger, D., Bradley, N., Edme, P., & Robertsson, J. O. A. (2023). Efficient wave type fingerprinting and filtering by six-component polarization analysis. *Geophysical Journal International*, *234*(1), 25–39. <https://doi.org/10.1093/gji/ggad071>
- Soret, L., Gérard, J. C., Montmessin, F., Piccioni, G., Drossart, P., & Bertaux, J. L. (2012). Atomic oxygen on the Venus nightside: Global distribution deduced from airglow mapping. *Icarus*, *217*(2), 849–855. <https://doi.org/10.1016/j.icarus.2011.03.034>
- Stähler, S. C., Khan, A., Banerdt, W. B., Lognonné, P., Giardini, D., Ceylan, S., et al. (2021). Seismic detection of the Martian core. *Science*, *373*(6553), 443–448. <https://doi.org/10.1126/science.abi7730>
- Stevenson, D., Cutts, J., MimounDavid, Arrowsmith, S., Banerdt, B., Blom, P., et al. (2015). *Probing the interior structure of Venus (Tech. Rep.)*. Keck Institute for Space Studies: Venus Seismology Study Team.
- Stolov, A., & OFS. (2019). Testing optical fiber: Undersea and downhole applications. Retrieved from https://www.photonics.com/Articles/Testing_Optical_Fiber_Undersea_and_Downhole/p5/v170/f1115/a64288
- Surkov, Y. A., Barsukov, V., Moskal'yeva, L., Kharyukova, V., & Kemurdzhian, A. (1984). New data on the composition, structure, and properties of Venus rock obtained by Venera 13 and Venera 14. *Journal of Geophysical Research*, *89*(S02), B393–B402. <https://doi.org/10.1029/jb089is02p0b393>
- Sutin, B. M., Cutts, J., Didion, A. M., Drilleau, M., Grawe, M., Helbert, J., et al. (2018). VAMOS: A SmallSat mission concept for remote sensing of Venusian seismic activity from orbit. In M. Lystrup, H. A. MacEwen, G. G. Fazio, N. Batalha, N. Siegler, & E. C. Tong (Eds.), *Space telescopes and instrumentation 2018: Optical, infrared, and millimeter wave* (Vol. 10698, p. 106985T). <https://doi.org/10.1117/12.2309439>
- Tian, Y., Herrick, R. R., West, M. E., & Kremic, T. (2023). Mitigating power and memory constraints on a Venusian seismometer. *Seismological Research Letters*, *94*(1), 159–171. <https://doi.org/10.1785/0220220085>
- Trahan, A. J., & Petculescu, A. (2020). Absorption of infrasound in the lower and middle clouds of Venus. *Journal of the Acoustical Society of America*, *148*(1), 141–152. <https://doi.org/10.1121/10.0001520>
- van Zelst, I. (2022). Comment on “Estimates on the frequency of volcanic eruptions on Venus” by Byrne & Krishnamoorthy (2022). *Journal of Geophysical Research: Planets*, *127*(12), e2022JE007448. <https://doi.org/10.1029/2022JE007448>
- van Zelst, I., Maia, J. S., Plesa, A.-C., Ghail, R., & Spühler, M. (2024). Estimates on the possible annual seismicity of Venus. *Journal of Geophysical Research: Planets*, *129*(7), e2023JE008048. <https://doi.org/10.1029/2023JE008048>
- Walter, F., Gräff, D., Lindner, F., Paitz, P., Köpfl, M., Chmiel, M., & Fichtner, A. (2020). Distributed acoustic sensing of microseismic sources and wave propagation in glaciated terrain. *Nature Communications*, *11*(1), 2436. <https://doi.org/10.1038/s41467-020-15824-6>
- Wang, H. F., Zeng, X., Miller, D. E., Fratta, D., Feigl, K. L., Thurber, C. H., & Mellors, R. J. (2018). Ground motion response to an ML 4.3 earthquake using co-located distributed acoustic sensing and seismometer arrays. *Geophysical Journal International*, *213*(3), 2020–2036. <https://doi.org/10.1093/gji/ggy102>
- Widemann, T., Straume-Lindner, A. G., Ocampo, A., Voirin, T., Carter, L., Hensley, S., et al. (2022). EnVision: A nominal science phase spanning six Venus sidereal days (four earth years). *AGU fall meeting abstracts*, *2022*, P55B-05.
- Wilson, C. F., Zetterling, C.-M., & Pike, W. T. (2016). Venus long-life surface package. In *White paper submitted in response to ESA's call for new scientific ideas*. arXiv e-prints, arXiv:1611.03365. <https://doi.org/10.48550/arXiv.1611.03365>
- Xu, Z., Broquet, A., Fuji, N., Kawamura, T., Lognonné, P., Montagner, J.-P., et al. (2023). Investigation of Martian regional crustal structure near the dichotomy using S1222a surface-wave group velocities. *Geophysical Research Letters*, *50*(8), e2023GL103136. <https://doi.org/10.1029/2023GL103136>
- Zhan, Z. (2020). Distributed acoustic sensing turns fiber-optic cables into sensitive seismic antennas. *Seismological Research Letters*, *91*(1), 1–15. <https://doi.org/10.1785/0220190112>
- Zharkov, V. N. (1983). Models of the internal structure of Venus. *The Moon and the Planets*, *29*(2), 139–175. <https://doi.org/10.1007/BF00928322>